High pressure melting of wüstite

Rebecca A. Fischer[1,2,*] and Andrew J. Campbell[1]

[1]Department of Geology, University of Maryland, College Park, Maryland 20742, U.S.A.

[2]Northwestern University, Evanston, Illinois 60208, U.S.A.

*Corresponding author: raf815@umd.edu

American Mineralogist, in press 2010

Abstract

Iron oxide (FeO) is an important component in the mineralogy of Earth's lower mantle, and possibly its core, so its phase diagram is essential to models of the planet's interior. The melting curve of wüstite, $Fe_{0.94}O$, was determined up to 77 GPa and 3100 K in a laser-heated diamond anvil cell. Melting transition temperatures were identified from discontinuities in the emissivity vs. temperature relationship within the laser-heated spot. The melting curve exhibits no obvious kinks that could be related to a subsolidus transition in wüstite, but there is evidence for a two-phase loop at pressures below 30 GPa. Comparison of these results to previous studies on Fe, Fe-O, and Fe-S confirms that the melting point depression in the Fe-O system remains significantly less, by a factor of 2 or more, than that in the Fe-S system up to pressures exceeding 80 GPa.

Introduction

Oxidized iron is an important component of rocks throughout the Earth's mantle, and it is possible that iron oxide is an alloying component in the Earth's core too (McDonough 2003). Furthermore, because Fe is the most abundant multivalent element in the mantle, its oxidation state dominates the redox chemistry of the mantle, in turn controlling element partitioning, phase equilibria, diffusion, and related physical and chemical properties (Frost and McCammon 2008). If oxygen is a primary light element component in the core, then its impact on the melting temperature and density of Fe-rich melts is essential to interpreting the dynamics and evolution of the core. Therefore, it is critical that we understand the phase relations and thermodynamics of the Fe-O system at high pressures and temperatures. In this study we focus on the melting curve in the iron oxide wüstite ($Fe_{1-x}O$).

At ambient conditions wüstite is stable in the B1 (NaCl) crystal structure, and with room temperature compression it undergoes a rhombohedral distortion at 17 GPa (Fei and Mao 1994). Diamond cell and shock wave results suggest a transformation to the B8 (NiAs) structure at high temperatures and approximately 70 GPa (Fei and Mao 1994; Jeanloz and Ahrens 1981; Knittle and Jeanloz 1991; Murakami et al. 2004; Kondo et al. 2004), based on X-ray diffraction and electrical conductivity measurements. However, the slope of the B1/B8 transition is inconsistent among these studies, and some investigators have failed to observe the phase change altogether, even at significantly higher pressures (Yagi et al. 1985; Sata et al. 2005; Seagle et al. 2008), perhaps related to differences in stoichiometry (Seagle et al. 2008). Previous investigations of the melting curve of $Fe_{1-x}O$ using a multi-anvil press

(Ringwood and Hibberson 1990) and diamond anvil cell (Boehler 1992; Shen et al. 1993) have been in reasonable agreement up to *P,T* conditions of about 50 GPa and 2700 K. An earlier diamond anvil cell study by Knittle and Jeanloz (1991) reported significantly higher melting temperatures, near 3800 K at 50 GPa. Recently Seagle et al. (2008) reported a single melting point for wüstite near 3100 K at 52 GPa, intermediate between the results of Knittle and Jeanloz (1991) and Shen et al. (1993).

In this study we aim to determine the melting curve of wüstite at high pressures, to resolve between existing discrepancies in the literature data and further clarify high pressure melting in the Fe-O binary. We additionally aim to extend the melting curve to higher pressures than previous studies, to allow for improved extrapolation to core pressures. To achieve these goals, we apply a new method for identifying phase transitions in laser-heated diamond anvil cell samples, based on the imaging radiometric technique of Campbell (2008).

Experimental Methods

Wüstite powder (Alfa Aesar) was ground to a grain size of ~1-5 μm. The lattice parameter *a* was measured by X-ray diffraction to be 4.302 Å, corresponding to a composition of $Fe_{0.94}O$ (McCammon and Liu 1984). The powder was pressed in a diamond anvil cell to form foils approximately 50-80 μm in diameter, and loaded into a symmetric-type diamond anvil cell with a small amount of ruby powder as a pressure standard (Mao et al. 1986). Argon was loaded cryogenically to serve as the pressure medium and thermal insulator. In two experiments KBr was used as the pressure medium instead; the KBr was

baked before use, and the sample assembly was also oven-dried after cell loading but before pressurization. A cross-section of the loaded cell is diagrammed in Appendix 1.

Pressurized samples were heated from one side with a 1064 nm Yb-doped fiber laser (IGP Photonics YLR-50-1064-LP). Heating lasted approximately 10 minutes per spot, with laser power gradually increased throughout heating, and several temperature measurements were made at each laser power. Samples were heated in 1-4 locations, with each spot heated only once. Errors in pressure are estimated as 1σ uncertainties based on measurements at multiple ruby markers within the sample chamber both before and after heating. Contributions from thermal pressure, likely to be <3 GPa at these *P,T* conditions in argon (Dewaele et al. 2007), are not included.

Temperature distributions were measured by multispectral imaging radiometry (Campbell 2008). Images of the laser-heated spot were collected simultaneously at 670, 750, 800, and 900 nm and spatially correlated (Campbell 2008). At each position, a four-color fit was made to the Planck radiation function using the graybody approximation (wavelength-independent emissivity), to construct the emissivity and temperature distributions in the spot in two dimensions (Figure 1). Figure 2 illustrates temperature-dependent variations in emissivity. Phase changes were identified by discontinuities in temperature-emissivity profiles across the central region of the hot spot (Figure 2), reflecting changes in the sample's optical properties through a phase transition (Campbell 2008). Appendix 2 shows temperature-emissivity profiles from a single experiment at various laser power settings. Discontinuities are not visible at lower laser powers before the melting point is reached, but appear at an invariant temperature at higher laser powers. The temperature range in each

profile was limited by the dynamic range of the CCD camera. This detection of melting was further supported by visual observations during heating, such as apparent movement within the laser spot, as well as changes in the sample's surface texture upon quench. For each experiment the temperature-emissivity discontinuities were identified in multiple temperature maps, at different laser powers. Each reported temperature is a mean calculated from 3-6 temperature maps, and from 3-7 distinct temperature-emissivity profiles across each map. Errors in temperature are one standard deviation of these values. Possible systematic errors, such as violations of the graybody approximation, are not included. In single-sided laser heating experiments thermal gradients also exist axially (through the thickness of the sample), but the temperature measurements and criteria for melting were both applied only to the surface of the sample, similar to previous studies (Knittle and Jeanloz 1991; Boehler 1992; Shen et al. 1993).

Results

The melting curve of wüstite is shown in Figure 3, and the pressure-temperature data obtained in this study are listed in Appendix 3. Our data define the melting curve in $Fe_{0.94}O$ to 77 GPa and 3100 K. The temperature vs. emissivity method (Figure 2) identifies the location of a phase change, but it provides no structural information; the nature of the phase change is determined by comparison to results obtained by other methods.

Figure 3 also includes a comparison between our data and several other previous studies. Ringwood and Hibberson (1990) established a melting point for FeO at 16 GPa, by

extrapolation of solid/melt (Mg,Fe)O compositions in their run products. Knittle and Jeanloz (1991), using the laser heated diamond anvil cell, identified melting by visual examination of the quenched sample, or observation of movement during heating. Their results lie at much higher temperatures than subsequent diamond cell studies. Boehler (1992) and Shen et al. (1993) presented melting curves of wüstite that are very similar to the present results; in fact the Boehler (1992) data, reaching 47 GPa, are indistinguishable from our data over that pressure range (Figure 3). The melting criteria applied by both Boehler (1992) and Shen et al. (1993) involved a combination of visual observation (aided by Ar^+ laser illumination) and changes in the laser power vs. temperature relationship during laser heating. Boehler (1992) used an Ar pressure medium, like the present study. Shen et al. (1993) used solid oxide media, which may cause an underestimate of pressure because of thermal contributions, possibly explaining the small offset between our data and those of Shen et al. (1993). Recently Seagle et al. (2008) used X-ray diffraction methods to place bounds on wüstite melting at 52 GPa; their lower bound lies approximately 200 K higher than our results (Figure 3). Unlike all earlier studies, we observe an additional transition along the melting curve below ~28 GPa, presumably a partial melting loop as discussed below.

At pressures of 55 GPa and above, we note that the high-pressure melting curve of argon (Boehler et al. 2001) passes through the data (Figure 3), raising the possibility that these measurements could be related to melting of the argon used as the pressure medium in these experiments. It is not obvious that melting of the transparent pressure medium should produce a measurable signal in the temperature vs. emissivity plots, but the coincidence of the data with Boehler et al.'s (2001) Ar melting curve deserves consideration. The two

measurements using a KBr pressure medium were a test of the data, to verify that the observed signal is melting of $Fe_{0.94}O$. The data obtained using a KBr medium are broadly consistent with the rest of the data (Figure 3), supporting our interpretation that the emissivity change is related to melting of the iron oxide. Note also that thermal pressure effects are not included in the reported pressures, and KBr, being a stiffer pressure medium than argon, should produce a several GPa thermal pressure increase, bringing those two data into even closer alignment with the argon-based data.

Discussion

This study uses the emissivity vs. temperature method described by Campbell (2008) to identify phase transitions in laser-heated spots. The principle is very similar to that applied in some earlier studies of melting, that used emissivity vs. temperature or temperature vs. laser power relationships to identify changes that occur between successive measurements (e.g., Boehler et al. 1990; Shen and Lazor 1995; Lord et al. 2009); the difference here is that the phase transition can be identified within a single measurement of the temperature distribution. The method works because the emissivity is a material property that may change as the material undergoes a phase transition. This emissivity change may be great or small, and can also be undetectable, depending on the nature of the specific phase transition involved. Other experimental factors can also cause optical changes (Jeanloz and Kavner 1996), so it is important to have anchored our results to independently determined phase transition *P,T* points (Ringwood and Hibberson 1990; Boehler 1992) (Figure 3).

The Lindemann Law is a vibrational-based model of melting that has broad empirical support, and requires knowledge of the high-*P,T* equation of state of a material for its implementation. We used the Lindemann Law formulation of Anderson and Duba (1997) to make a prediction of melting of wüstite at high pressures, and applied the bulk modulus, Grüneisen parameter, and other equation of state parameters determined for stoichiometric FeO (Campbell et al. 2009) to the wüstite phase in the present study, changing only the initial volume to accommodate the stoichiometric difference. This is supported by previous work (Fei 1996) showing no change in bulk modulus with stoichiometric parameter x in $Fe_{1-x}O$. The resulting Lindemann melting curve, shown in Figure 3, passes slightly below the present results, reaching a 160 K difference from our data at the maximum pressure of 78 GPa. This is reasonable agreement given the empirical nature of the law, and the uncertainty in the equation of state for the $x = 0.06$ phase. The Lindemann prediction obtains a more exact fit to our data if the Grüneisen parameter of $Fe_{0.94}O$ is chosen as $\gamma_0 = 1.52$ instead of the $Fe_{1.00}O$ value of 1.42 (Campbell et al. 2009). With this parameter, the extrapolated melting point of $Fe_{0.94}O$ at the core-mantle boundary pressure (136 GPa) is 3690 K, and at the inner core boundary pressure (330 GPa) it is 4600 K.

This extrapolation of the melting curve to high pressures presumes, of course, that no phase transition appears along the solidus to cause a kink in its slope. The B1/B8 phase transition would be expected to do just that, although the pressure at which this occurs is uncertain because of conflicting reports of its slope, as discussed in the Introduction. Knittle and Jeanloz (1991) and Fei and Mao (1994) anticipated a B1/B8/melt triple point near 70 GPa, but the B1/B8 slope reported by Kondo et al. (2004) would cross our melting curve

close to 300 GPa. Others (Sata et al. 2005; Seagle et al. 2008) saw no B8 phase transition in wüstite. There is no obvious kink along the melting curve within the pressure range examined here, although a small kink might be obscured by the uncertainty of the data.

At lower pressures, in the approximate range 10 to 25 GPa, the optical method used to determine phase transitions appeared to recognize two distinct boundaries, separated by 50-200 K (Figure 3). The measured temperatures are 400-800 K higher than the reported melting curve of Ar (Boehler et al. 2001), so the observed signal is not melting of the pressure medium. The optically determined transitions appear to form a loop here, so the simplest interpretation is that we have recorded a two-phase partial melting loop in this *P,T* range for wüstite. Additional support for this interpretation comes from visual observation of the sample, in which a hole sometimes appeared after crossing the lower boundary of the loop. Melting at other pressures in the Figure 3 phase diagram may occur either congruently or over a narrow phase loop, unresolved in our experiments. Previous studies (Boehler 1992; Shen et al. 1993) may not have observed this loop because of the resolution of their melting criteria. Alternatively, it is possible that the lower transition temperature in this range represents a previously unobserved subsolidus transition in $Fe_{0.94}O$, although this would not easily explain the creation of holes sometimes observed in those samples. Another scenario that we cannot strictly exclude is that one of the boundaries describing this loop is an experimental artifact, derived from an optical or physical change that is unrelated to a phase transition in the sample material. However, the observed, limited pressure range would seem unlikely in this case, and we conclude that a phase loop below the liquidus is the most likely explanation of the data in the 10 to 25 GPa range. Further structural and/or phase information

obtained by X-ray diffraction or quench studies would be useful to clarify the behavior of wüstite in this pressure-temperature range.

Comparisons between this work and the recent work of Seagle et al. (2008) have implications for the interpretation of those data. Seagle et al. (2008) used synchrotron X-ray diffraction to determine melting in the Fe-FeO binary system; in this method the temperatures are measured on the surface of the sample, but the melting point is determined by disappearance of crystalline phase(s) throughout the thickness of the sample. Therefore, there is a possibility of systematic bias in the temperature measurements, if the center of the sample is cooler than the heated surfaces. (With increasing pressure, the sample thins and the axial gradient should diminish.) Seagle et al. (2008) refer to the large disagreement at ~50 GPa between the melting points of $Fe_{0.94}O$ (Figure 3), and add their X-ray diffraction results bounding the melting point between 3030 ± 150 K and 3220 ± 150 K at 52 GPa. Our new data show that the melting point at 51 GPa is 2814 ± 43 K (at 52 GPa it is ~12 K higher). In the new method used here, the temperatures are measured from exactly the same sample signal from which melting is determined, so that measurement bias is eliminated and we expect these results to be more accurate.

A further comparison is made in Figure 2 between the present results and the measurements of Seagle et al. (2008). We analyzed the temperature measurement data obtained during the 52 GPa laser-heating experiments in the Seagle et al. (2008) study, to compare directly the temperature vs. emissivity relationship in those experiments to those of the present study. (The temperature-emissivity data from Seagle et al.(2008) correspond to different points in time at the same location, a 5 μm region centered in the hotspot, whereas

our temperature-emissivity profiles reflect different locations within the hotspot at the same moment in time.) The results (Figure 2) are similar; the Seagle et al. (2008) emissivities exhibit a kink near 2750 K, within uncertainty of our melting point at 51 GPa, although the X-ray diffraction data of Seagle et al. (2008) associated with these measurements do not reveal the loss of B1-FeO diffraction peaks until above 3030 K. This observation indicates that the samples behaved similarly in the two sets of experiments, and is consistent with our conclusion, supported by thermal modelling of the laser heated sample (Campbell et al. 2007), that the temperature gradient through the thickness of the sample must be carefully considered when interpreting X-ray diffraction results.

Therefore, our results indicate that the Seagle et al. (2008) study likely overestimated the 52 GPa melting temperature of wüstite by ~200 K. Assuming that this estimate can be applied to all samples in that study, then the eutectic depression in the Fe-FeO system, relative to the pure Fe melting curve of Shen et al. (1998), is approximately 450 K in the 20 and 90 GPa pressure ranges, and reduces to ~200 K in the vicinity of 70 GPa because of the fcc/hcp phase transition in Fe. In contrast, in the Fe-S system the eutectic depression of the melting point is 700-900 K up to at least 80 GPa (Campbell et al. 2007). If this difference in melting point depressions persists to core pressures, an Fe-O core may require higher temperatures than an Fe-S core. Furthermore, for any model of cooling history an Fe-O core will crystallize more quickly and could drive convection by compositional buoyancy more efficiently than an Fe-S core would.

Acknowledgments

We are grateful to Noah Miller, Gregory Shofner, and Tess Van Orden for technical assistance, to Peter Zavalij for X-ray diffraction analysis of the starting material, and to Chris Seagle for generously providing the unprocessed temperature measurement data from a previous study. This work was supported by NSF grant EAR-0635722, including an REU supplement supporting R.A.F.

References

Anderson, O. L., and A. Duba (1997), Experimental melting curve of iron revisited, *J. Geophys. Res., 102*, 22659-22669.

Boehler, R. (1992), Melting of the Fe-FeO and the Fe-FeS systems at high pressure – constraints on core temperatures, *Earth Planet. Sci. Lett., 111*, 217-227.

Boehler, R., N. von Bargen, and A. Chopelas (1990), Melting, thermal expansion, and phase transitions of iron at high pressures, *J. Geophys. Res., 95,* 21731-21736.

Boehler, R., M. Ross, P. Söderline, and D. B. Boercker (2001), High-pressure melting curves of argon, krypton, and xenon: Deviation from corresponding states theory, *Phys. Rev. Lett., 86,* 5731-5734.

Campbell, A. J. (2008), Measurement of temperature distributions across laser-heated samples by multispectral imaging radiometry, *Rev. Sci. Instrum., 79*, 015108.

Campbell, A. J., C. T. Seagle, D. L. Heinz, G. Shen, and V. B. Prakapenka (2007), Partial melting in the iron-sulfur system at high pressure: A synchrotron X-ray diffraction study, *Phys. Earth Planet. Inter., 162,* 119-128.

Campbell, A. J., L. Danielson, K. Righter, C. T. Seagle, Y. Wang, and V. B. Prakapenka (2009), High pressure effects on the iron-iron oxide and nickel-nickel oxide oxygen fugacity buffers, (submitted).

Darken, L. S., and R. W. Gurry (1946), The system iron-oxygen, II, Equilibrium and thermodynamics of liquid oxides and other phases, *J. Am. Chem. Soc., 68*, 798-816.

Dewaele, A., M. Mezouar, N. Guignot, and P. Loubeyre (2007), Melting of lead under high pressure studied using second-scale time-resolved x-ray diffraction, *Phys. Rev. B., 76,* 144106.

Fei, Y. (1996), Crystal chemistry of FeO at high pressures and temperatures, in: Dyar, M. D., C. McCammon, and M. W. Shaefer (Eds.), *Mineral Spectroscopy: A Tribute to Roger Burns*. Geochemical Society, Houston, pp. 243-254.

Fei, Y., and H.-k. Mao (1994), In-situ determination of the NiAs phase of FeO at high-pressure and temperature, *Science, 266*, 1678-1680.

Frost, D. J., and C. A. McCammon (2008), The redox state of Earth's mantle, *Annu. Rev. Earth Planet. Sci., 36*, 389-420.

Jeanloz, R., and T. J. Ahrens (1980), Equations of state of FeO and CaO, *Geophys. J. R. astr. Soc., 62,* 505-528.

Jeanloz, R., and A. Kavner (1996), Melting criteria and imaging spectroradiometry in laser-heated diamond-anvil cell experiments, *Phil. Trans. R. Soc. London A, 354,* 1279-1305.

Knittle, E., and R. Jeanloz (1991), The high-pressure phase diagram of $Fe_{0.94}O$: A possible constituent of the Earth's core, *J. Geophys. Res., 96*, 16169-16180.

Kondo, T., E. Ohtani, N. Hirao, T. Yagi, and T. Kikegawa (2004), Phase transitions of (Mg,Fe)O at megabar pressures, *Phys, Earth Planet. Inter., 143-144*, 201-213.

Lord, O., M. J. Walter, R. Dasgupta, D. Walker, and S. M. Clark (2009), Melting in the Fe-C system to 70 GPa, *Earth Planet. Sci. Lett., 284*, 157-167.

Mao, H.-K., J. Xu, and P. M. Bell (1986), Calibration of the ruby pressure gauge to 800 kbar under quasi-hydrostatic conditions, *J. Geophys. Res., 91,* 4673-4676.

McCammon, C. A., and L.-g. Liu (1984), The effects of pressure and temperature on non-stoichiometric wüstite, Fe_xO: The iron-rich phase boundary, *Phys. Chem. Minerals, 10,* 106-113.

McDonough, W. F. (2003), Compositional model for the Earth's core, in: Carlson, R. W. (Ed.), *Treatise of Geochemistry, Vol. 2*. Elsevier Ltd., pp. 547-568.

Murakami, M., K. Hirose, S. Ono, T. Tsuchiya, M. Isshiki, and T. Watanuki (2004), High pressure and high temperature phase transitions of FeO, *Phys. Earth Planet. Inter., 146*, 273-282.

Ringwood, A. E., and W. Hibberson (1990), The system Fe-FeO revisited, *Phys. Chem. Miner., 17,* 313-319.

Sata, N., K. Hirose, Y. Oshino, and G. Shen (2005), High-pressure experiments on FeO up to 200 GPa, *EOS Trans. AGU, 86,* Fall Meet. Suppl., Abstract MR31A-0124.

Seagle, C. T., D. L. Heinz, A. J. Campbell, V. B. Prakapenka, and S. T. Wanless (2008), Melting and thermal expansion in the Fe-FeO system at high pressure, *Earth Planet. Sci. Lett., 265*, 655-665.

Shen, G., and P. Lazor (1995), Measurement of melting temperatures of some minerals under lower mantle pressures, *J. Geophys. Res., 100,* 17699-17713.

Shen, G., P. Lazor, and S. K. Saxena (1993), Melting of wüstite and iron up to pressures of 600 kbar, *Phys. Chem. Minerals, 20,* 91-96.

Shen, G., H.-k. Mao, R. J. Hemley, T. S. Duffy, and M. L. Rivers (1998), Melting and crystal structure of iron at high pressures, *Geophys. Res. Lett., 25*, 373-376.

Yagi, T., K. Suzuki, and S. Akimoto (1985), Static compression of wüstite ($Fe_{0.98}O$) to 120 GPa, *J. Geophys. Res., 90,* 8784-8788.

Figure Captions

Figure 1. Two-dimensional temperature map of a laser-heated spot at 21.5 GPa. Temperatures were determined by multispectral imaging radiometry (Campbell 2008), spatially correlating four images of the spot recorded simultaneously at different wavelengths and fitting each pixel to the Planck radiation function.

Figure 2. Representative temperature-emissivity profiles of laser-heated spots showing melting transitions during experiments at various pressures. Discontinuities in these plots, indicated by arrows, reflect abrupt changes in the samples' optical properties that accompany these transitions. Open and gray symbols denote opposing sides of the transect across the laser heated spot. Circles: 21 GPa; squares: 51 GPa; diamonds: 67 GPa. Green squares: results from the X-ray diffraction experiments of Seagle et al. (2008), showing temperature-emissivity data from sequential measurements on a sample at 52 GPa.

Figure 3. Melting curve of wüstite, $Fe_{0.94}O$. Solid circles: this study (argon pressure medium); shaded circles: this study (KBr medium); thick gray line: Lindemann Law prediction of $Fe_{0.94}O$ melting; solid purple line: $Fe_{0.96}O$ melting curve of Boehler (1992); dotted brown line: Ar melting curve of Boehler et al. (2001); dot-dashed blue line: $Fe_{0.94}O$ melting curve of Knittle and Jeanloz (1991); dashed green line: wüstite melting curve of Shen et al. (1993); open circle: 1 bar melting point of Darken and Gurry (1946); open

diamond: multi-anvil press melting study from Ringwood and Hibberson (1990); open triangles: bounds on melting from Seagle et al. (2008).

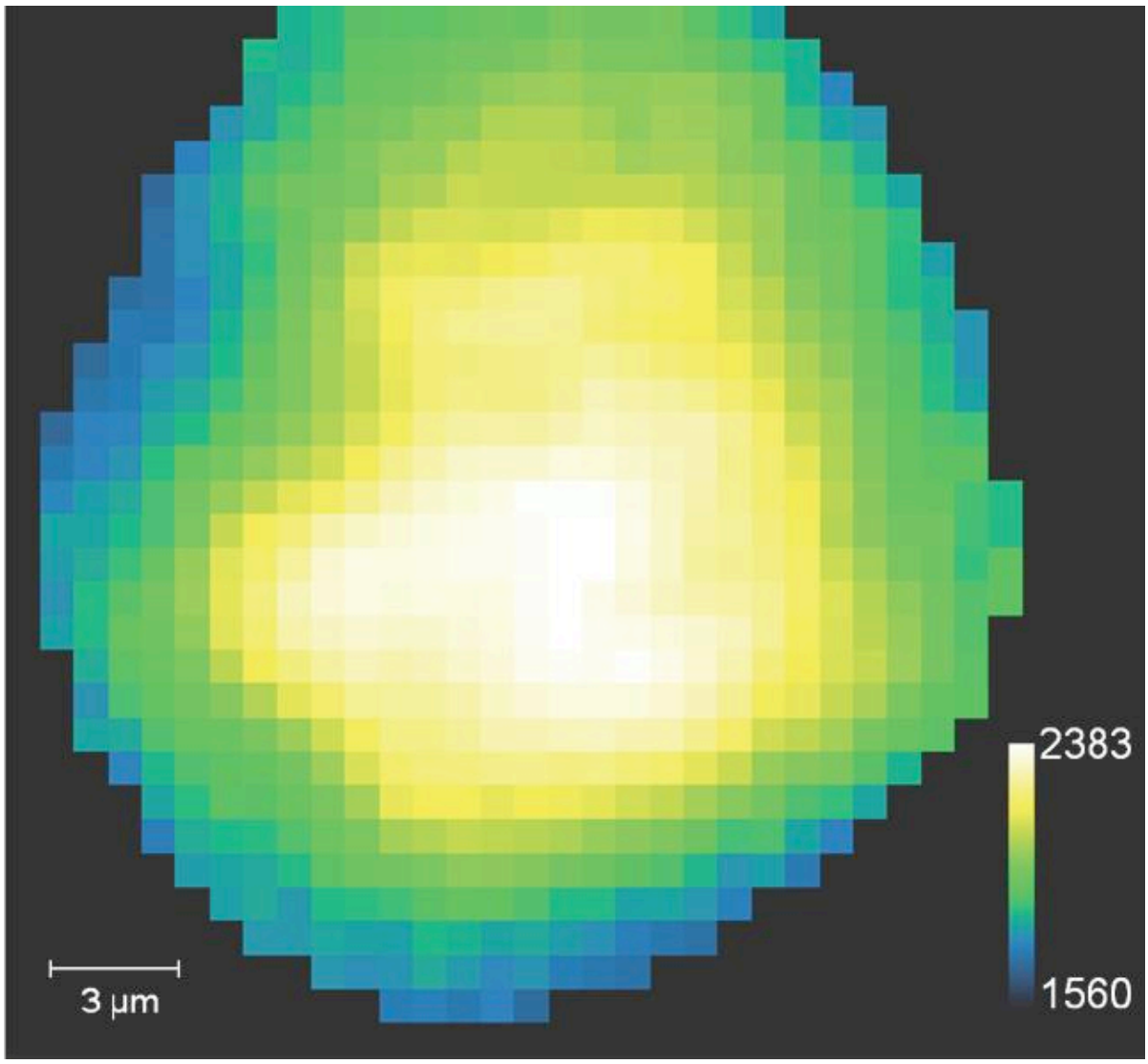

Figure 1

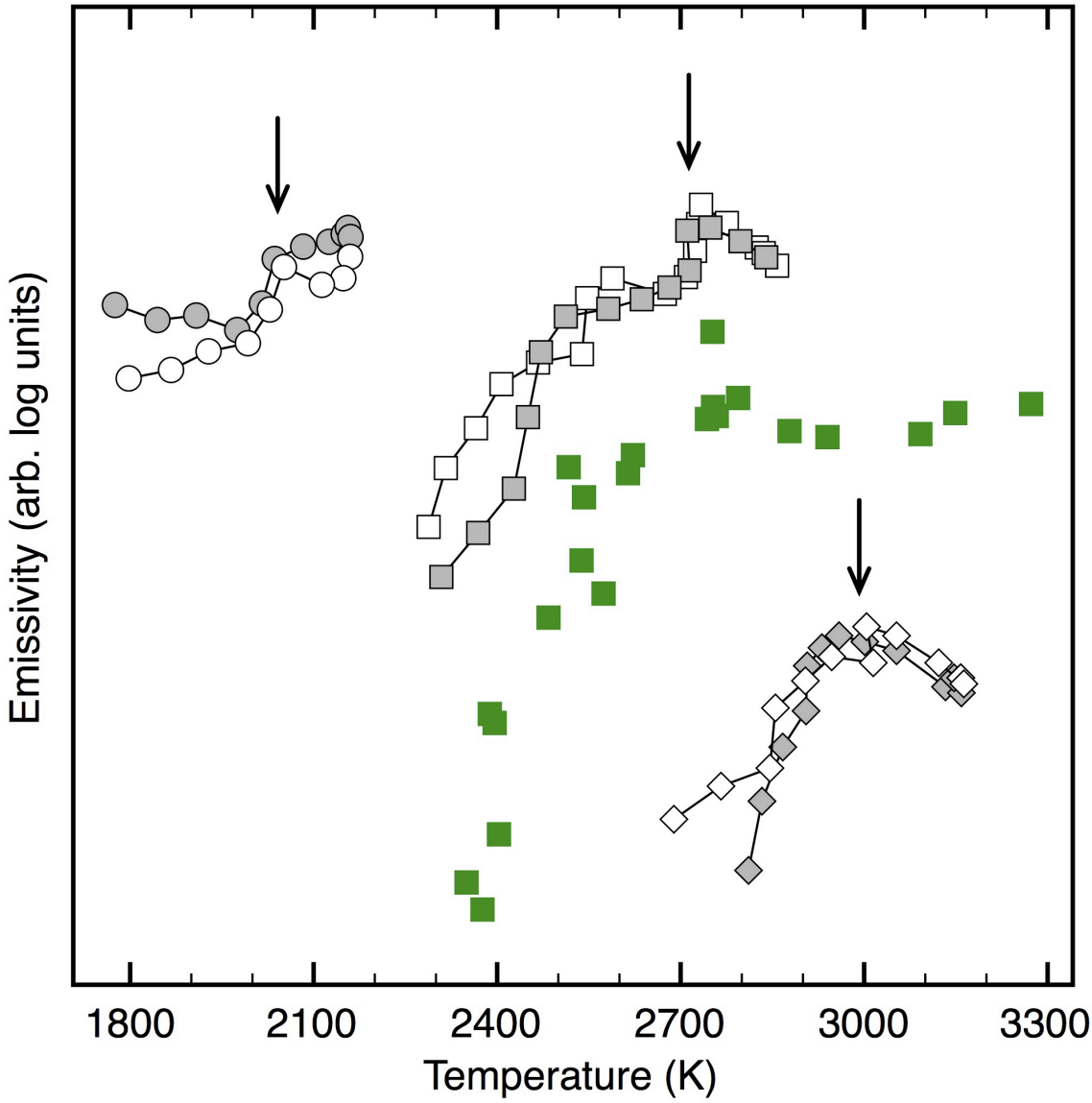
Emissivity (arb. log units)
1800
2100
2400
2700
3000
3300
Temperature (K)

Figure 2

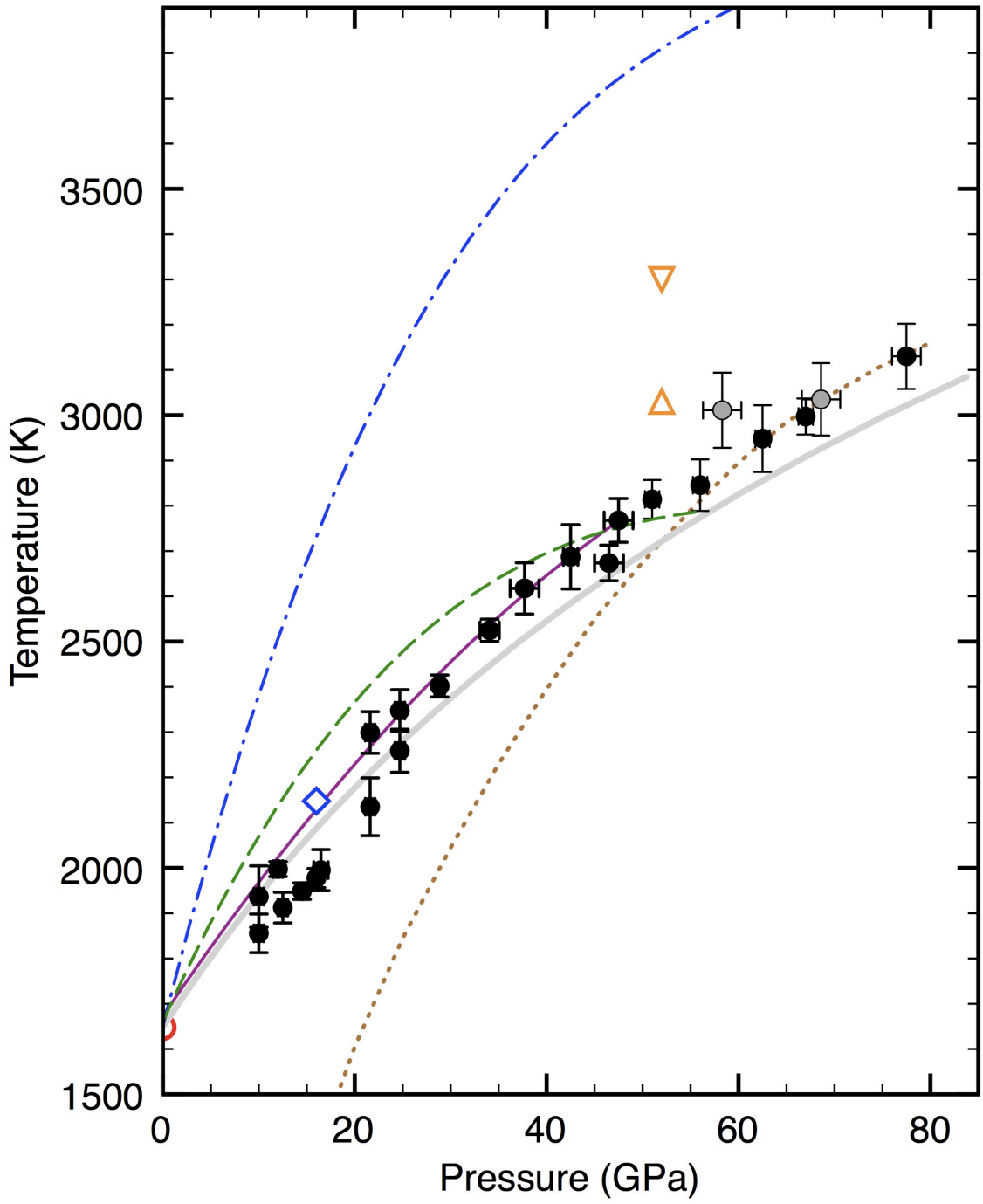
Temperature (K)
3500
3000
2500
2000
1500
0
20
40
60
80
Pressure (GPa)

Figure 3

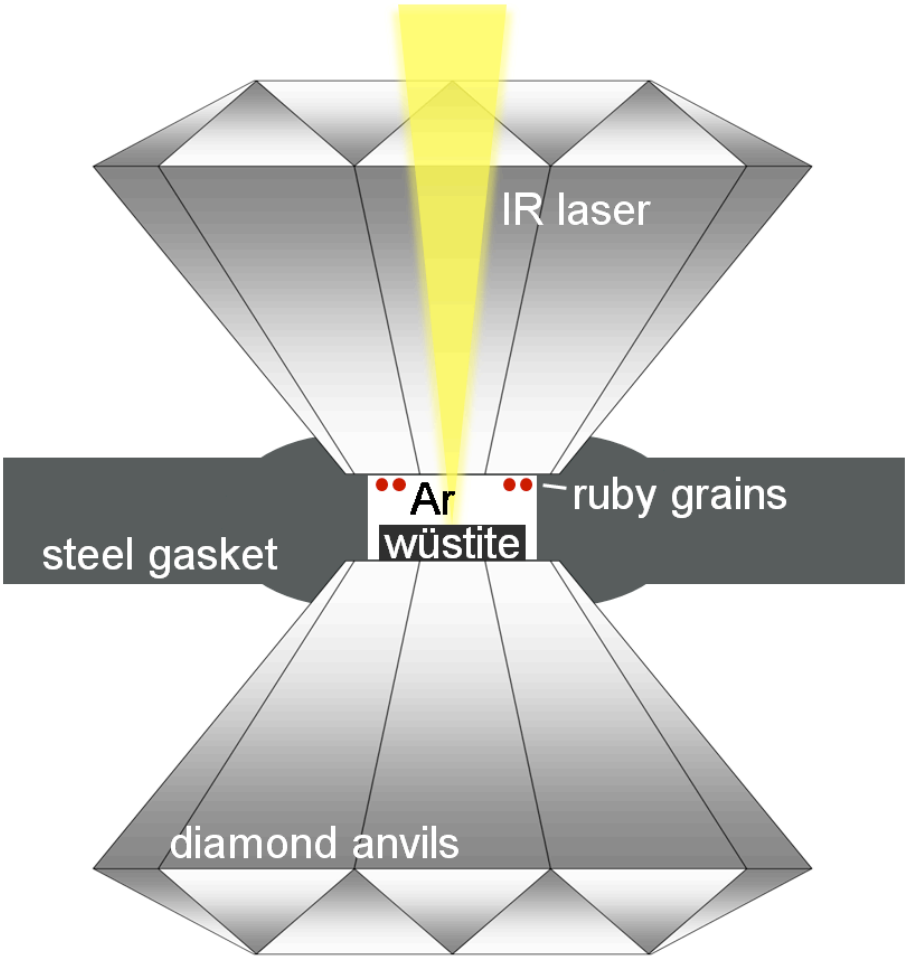

Appendix 1. Cross-sectional view of the diamond anvil cell and sample chamber. A thin wüstite pellet was laser heated on one side in an Ar environment. Pressures were determined by the ruby fluorescence method.

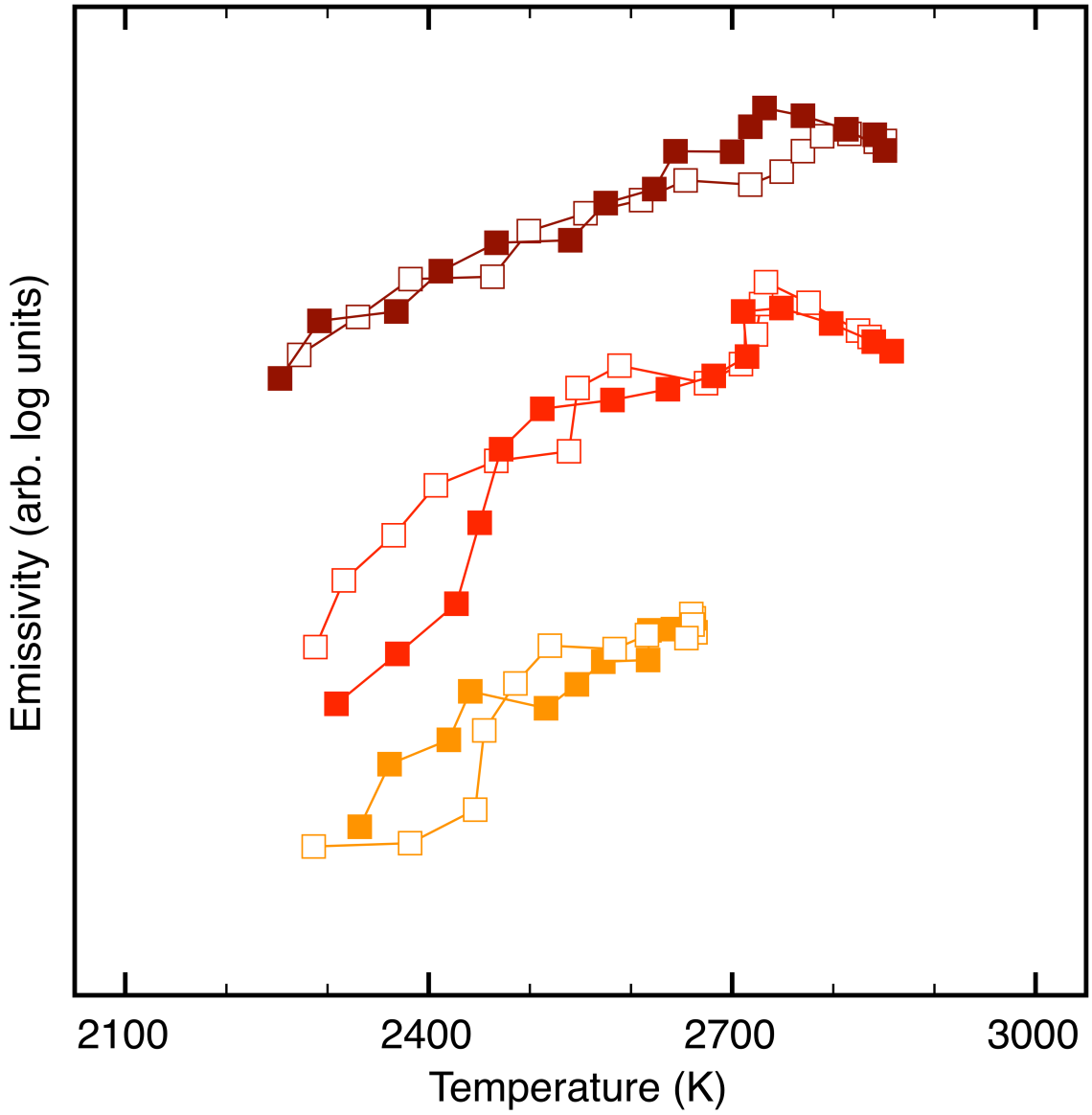

Appendix 2. Temperature-emissivity profiles from a single experiment at 51 GPa and different laser power settings. At lower laser powers (orange squares, 12.1 W laser output), before the melting point is reached, the melting-induced discontinuity is not evident in the profile. At higher laser powers (red squares, 15.6 W; maroon squares, 17.1 W), a discontinuity representing melting appears at the same temperature at various laser power

settings. Open and filled symbols represent opposing sides of the transect across the laser heated spot.

Appendix 3. Melting temperatures of wüstite, $Fe_{0.94}O$.

P (GPa)	sigma P	T (K)	sigma T
10.0	0.5	1856	43
10.0	0.5	1937	68
12.0	0.5	1998	17
12.5	0.5	1912	34
14.5	0.5	1949	18
16.0	0.5	1978	21
16.5	0.8	1995	45
21.6	0.5	2299	46
21.6	0.5	2135	64
24.7	0.5	2348	46
24.7	0.5	2259	48
28.8	0.5	2402	24
34.1	1.0	2525	25
37.7	1.5	2617	57
42.5	0.8	2687	71
46.5	1.5	2674	39
47.5	1.5	2768	48
51.0	0.8	2814	43
56.0	0.8	2845	57
62.5	0.8	2948	74
67.0	0.8	2997	40
77.5	1.5	3130	72